Mineralogical Magazine, June 2017, Vol. 81(3), pp. 485–498

Iyoite, $MnCuCl(OH)_3$ and misakiite, $Cu_3Mn(OH)_6Cl_2$: new members of the atacamite family from Sadamisaki Peninsula, Ehime Prefecture, Japan

D. Nishio–Hamane[1,*], K. Momma[2], M. Ohnishi[3], N. Shimobayashi[4], R. Miyawaki[2], N. Tomita[5], R. Okuma[1], A. R. Kampf[6] and T. Minakawa[5]

[1] Institute for Solid State Physics, the University of Tokyo, Kashiwa, Chiba 277-8581, Japan
[2] Department of Geology and Palaeontology, National Museum of Nature and Science, Tsukuba 305-0005, Japan
[3] 12-43 Takehana Ougi-cho, Yamashina-ku, Kyoto 607-8082, Japan
[4] Department of Geology and Mineralogy, Graduate School of Science, Kyoto University, Kitashirakawa Oiwake-cho, Sakyo-ku, Kyoto 606-8502, Japan
[5] Department of Earth Science, Faculty of Science, Ehime University, Matsuyama, Ehime 790-8577, Japan
[6] Mineral Sciences Department, Natural History Museum of Los Angeles County, 900 Exposition Boulevard, Los Angeles, CA 90007, USA

[*Received 31 August 2015; Accepted 29 March 2016; Associate Editor: Michael Rumsey*]

ABSTRACT

Two new members of the atacamite family were discovered recently in the Sadamisaki Peninsula, Ehime Prefecture, Japan. Iyoite, $MnCuCl(OH)_3$, is an Mn-Cu ordered analogue of botallackite, while misakiite, $Cu_3Mn(OH)_6Cl_2$, is an Mn-rich analogue of kapellasite. Both minerals occur in manganese ore crevices in close association with one another. Iyoite forms radial and dendritic aggregates consisting of pale green, bladed crystals. Misakiite commonly exists in emerald green, tabular, hexagonal crystals. The densities of iyoite and misakiite were calculated to be 3.22 and 3.42 g cm^{-3} based on their empirical formulae and powder X-ray diffraction data. Under the same axial setting of botallackite, iyoite is monoclinic, space group $P2_1/m$, a = 5.717(2), b = 6.586(2), c = 5.623(3) Å, β = 88.45(3)° and V = 211.63(15) $Å^3$. Misakiite is trigonal, space group $P\bar{3}m1$, with a = 6.4156(4), c = 5.7026(5) Å and V = 203.27(3) $Å^3$. The structures of both minerals are classified as layer type and the two are closely related. These new minerals were formed by the reaction between seawater and naturally-occurring manganese ores including native copper. These minerals are challenging to produce synthetically. Misakiite was synthesized successfully using a hydrothermal method, while iyoite could not be made.

Keywords: iyoite, misakiite, Mn-Cu ordering, atacamite family, new minerals, crystal structures, mineral synthesis, Sadamisaki Peninsula, Ehime Prefecture, Japan.

Introduction

The atacamite family contains two possible stoichiometries, $M^{2+}_2Cl(OH)_3$ and $Cu_3M^{2+}(OH)_6Cl_2$, where M^{2+} is Cu, Zn, Mg, Ni, Co, Fe or Mn. The first stoichiometry corresponds to the atacamite-, botallackite- and clinoatacamite-type structural polymorphs. Although M^{2+} in these minerals is typically Cu, kempite (M^{2+} = Mn) and hibbingite (M^{2+} = Fe) are also atacamite-type polymorphs. The $Cu_3M^{2+}(OH)_6Cl_2$ series consists of paratacamite-, herbertsmithite- and kapellasite-type polymorphs. The cations in the M^{2+} sites of these materials are commonly Zn, Ni, Co and Mg. Members of the atacamite family occur commonly as secondary minerals in copper-bearing ore. At present, 14 species in the atacamite family have been identified: atacamite, kempite, hibbingite,

*E-mail: hamane@issp.u-tokyo.ac.jp
https://doi.org/10.1180/minmag.2016.080.104

FIG. 1. Micrographs of iyoite and misakiite: (*a*) a radial aggregate of iyoite; (*b*) a hexagonal misakiite grain; (*c*) dendritic iyoite with hexagonal misakiite; (*d*) the apex of an iyoite dendrite with bladed misakiite. The field of view is 0.5 mm for (*a–c*) and 0.3 mm for (*d*).

botallackite, clinoatacamite, paratacamite, paratacamite-(Mg), paratacamite-(Ni), herbertsmithite, gillardite, leverettite, tondiite, kapellasite and haydeeite (Rogers, 1924; Fleet, 1975; Hawthorne, 1985; Parise and Hyde, 1986; Saini-Eidukat *et al*., 1994; Grice *et al*., 1996; Braithwaite *et al*., 2004; Krause *et al*., 2006; Clissold *et al*., 2007; Malcherek and Schlüter, 2007; Kampf *et al*., 2013*a*; Kampf *et al*., 2013*b*; Sciberras *et al*., 2014; Malcherek *et al*., 2014).

In 2013, during a mineralogical survey of the copper-manganese deposits located on the Sadamisaki Peninsula, Ehime Prefecture, Japan, one of the authors (D. N-H.) collected several atacamite-like minerals. Preliminary investigation revealed that these materials contained significant amounts of Mn; and botallackite-type $MnCuCl(OH)_3$ and kapellasite-type $Cu_3Mn(OH)_6Cl_2$ were identified subsequently as new minerals. Historically, Ehime Prefecture and the Sadamisaki Peninsula have been referred to colloquially as 'Iyo' and 'Misaki', respectively. The Sadamisaki Peninsula faces the Sea of Iyo and the Sea of Misaki. Hence $MnCuCl(OH)_3$ and $Cu_3Mn(OH)_6Cl_2$ have been named iyoite and misakiite, respectively. The minerals and their names have been approved by the International Mineralogical Association, Commission on New Minerals, Nomenclature and Classification (2013-130 for iyoite and 2013-131 for misakiite). The holotype specimen containing both minerals is deposited in the collections of the National Museum of Nature and Science, Japan, specimen number NSM–M43864. A cotype specimen is housed in the collections of the Mineral Sciences Department, Natural History Museum of Los Angeles County, Los Angeles, USA, catalogue number 66265.

Occurrence

The Sadamisaki Peninsula extends for 40 km from east to west and between 2 and 3 km from north to south. It is located on the westernmost part of Shikoku, one of the four main islands of Japan. This narrow peninsula faces the Sea of Iyo (north

https://doi.org/10.1180/minmag.2016.080.104 Published online by Cambridge University Press

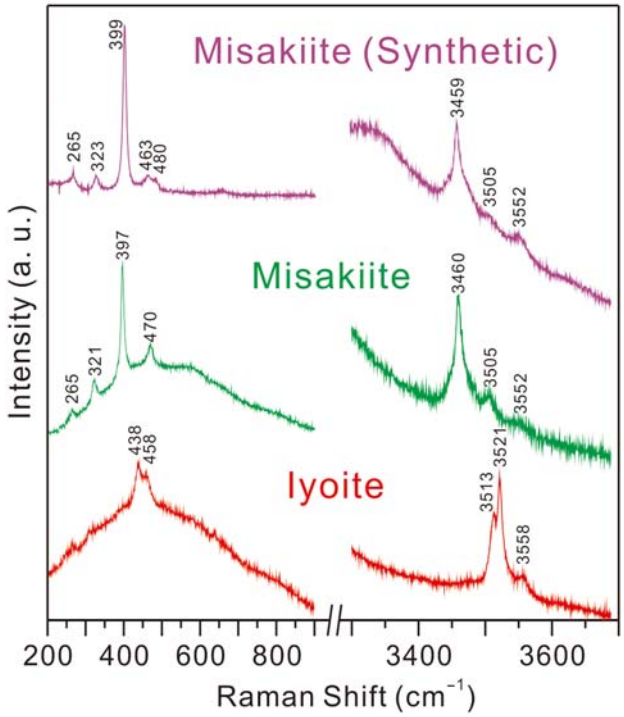

FIG. 2. Raman spectra of iyoite and misakiite.

side) and the Sea of Misaki (south side) and is situated in Ehime Prefecture. The rocks of this peninsula consist primarily of greenschists, with small amounts of piemontite schist included in the greenschists in some places. These materials belong to the Sambagawa metamorphic belt, which also contains Kieslarger-type deposits. These deposits are also called Besshi-type deposits, and were formed as volcanogenic massive sulfide deposits on the deep-sea floor of the Panthalassa Ocean in Late Jurassic times (e.g. Nozaki *et al*., 2013). A number of small-scale copper and manganese mines are scattered along the peninsula, and the Oku mine was once a small operation targeting copper-manganese deposits in association with the Besshi-type deposits. The mine was located near the coast (33°24′42″N 132°10′52″E), and the stratum consisting of the greenschist with piemontite schists continues into the sea. Rocks including masses of ore of varying size were scattered on the beach, and were exposed to seawater. The primary ore minerals in this area are hausmannite, tephroite, alleghanyite, rhodonite, rhodochrosite, native copper and chalcocite. The ore has been altered by reaction with seawater to produce secondary minerals of the atacamite family as well as cuprite, kutnohorite, malachite and chrysocolla. The new minerals are quite rare, and have not been found to co-exist with other members of the atacamite family.

Physical and optical properties

Iyoite and misakiite were found in crevices of manganese ore in close association with one another (Fig. 1). Iyoite is pale green in colour and forms radial and dendritic aggregates consisting of {001}, {100}, {010} and {110} bladed crystals, flattened on [001] and elongated parallel to [010]. These blades are typically 100–200 μm long. Iyoite dendritic aggregates are often accompanied by misakiite at the front edge of the aggregate (Fig. 1). Iyoite is transparent, brittle, with a tendency to fracture unevenly and has a vitreous lustre. It is optically biaxial (–) with α = 1.698(2), β = 1.725(3), γ = 1.737(3) (white light), $2V_{meas}$ = 66(2)° and $2V_{calc}$ = 66.5°. Dispersion is $r > v$, strong. Orientation is $Y = b$ and $X \wedge c^* = 26°$. It exhibits pleochroism with X (light bluish green) < Y (bluish green) ≈ Z (bluish green). The density

https://doi.org/10.1180/minmag.2016.080.104 Published online by Cambridge University Press

TABLE 1. Chemical compositions of iyoite and misakiite.

Constituent	Iyoite Mean of 7 grains (range)	Ideal[1]	Misakiite Mean of 7 grains (range)	Ideal[2]	Synthetic misakite Mean of 5 grains (range)
MnO	37.78 (36.79–40.86)	34.61	19.82 (18.32–20.26)	16.95	19.69 (18.69–20.42)
CuO	35.74 (32.09–36.13)	38.81	53.49 (53.30–55.30)	57.02	52.59 (51.26–54.38)
Cl	18.42 (17.90–18.93)	17.30	17.72 (17.48–17.83)	16.94	18.47 (17.87–19.07)
H_2O	13.01	13.18	12.65	12.91	12.22
O = Cl	–4.16	–3.90	–4.00	–3.82	–4.17
Total	100.79	100	99.68	100	98.80
	4 anions pfu		8 anions pfu		8 anions pfu
Mn	1.085		1.174		1.183
Cu	0.915		2.826		2.817
Cl	1.058		2.100		2.219
OH	2.942		5.900		5.781

[1]Calculated for the ideal formula $MnCuCl(OH)_3$; [2]Calculated for the ideal formula $Cu_3Mn(OH)_6Cl_2$
pfu – per formula unit.

calculated for iyoite using the empirical formulae and powder cell parameter is 3.22 g cm^{-3}.

Misakiite is emerald green in colour, and occurs as hexagonal plates 20–50 μm in diameter, flattened on {001} and bounded by {110} (Fig. 1). Misakiite also occurs as bladed crystals elongated parallel to [100], and these are often found at the ends of iyoite dendrites. Misakiite is transparent, brittle, with a tendency to fracture unevenly and has a vitreous lustre. It is optically uniaxial (–) with ω = 1.770(3) and ε = 1.750(3) (white light) and slight pleochroism: *O* (green-blue) > *E* (light green-blue). The density calculated using the empirical formulae and powder cell parameters is 3.42 g cm^{-3}.

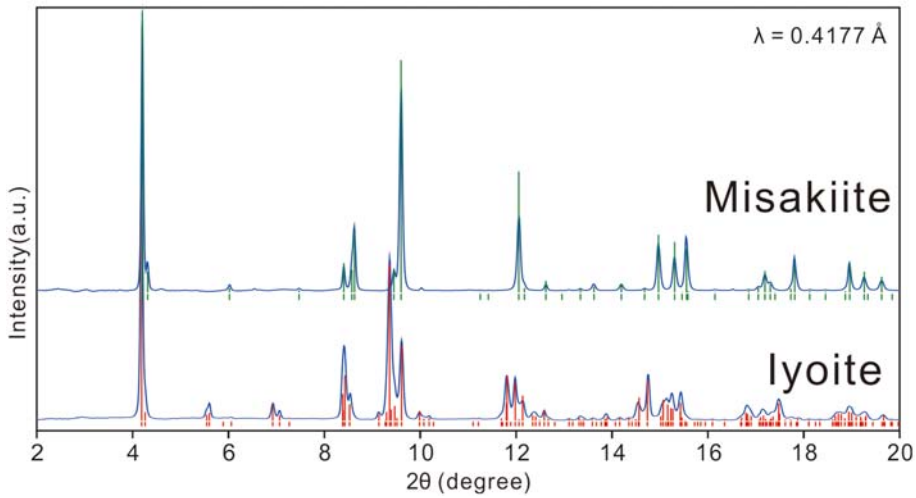

FIG. 3. Powder X-ray diffraction patterns of iyoite and misakiite. Bars below the diffraction lines indicate peak positions with intensities calculated from a single-crystal study.

https://doi.org/10.1180/minmag.2016.080.104 Published online by Cambridge University Press

TABLE 2. Powder X-ray diffraction data for iyoite and misakiite.

Iyoite					Misakiite				
I/I_0	$I_{calc.}$	$d_{obs.}$ (Å)	$d_{calc.}$ (Å)	*h k l*	I/I_0	$I_{calc.}$	$d_{obs.}$ (Å)	$d_{calc.}$ (Å)	*h k l*
100	100	5.7155	5.7152	100	100	100	5.7024	5.7026	001
12	3	5.6214	5.6211	001	11	3	5.5544	5.5561	100
3	2	4.3181	4.3163	110	2	2	3.9796	3.9795	101, 011
6	2	4.2735	4.2753	011	1	<1	3.2068	3.2078	110
	<1		4.0628	101	9	4	2.8510	2.8513	002
	<1		3.9546	$10\bar{1}$	12	7	2.7961	2.7958	111
6	5	3.4575	3.4577	111	24	6	2.7779	2.7780	200
3	2	3.3900	3.3902	$11\bar{1}$	7	6	2.5368	2.5367	102, 012
1	<1	3.3013	3.2926	020	76	58	2.4971	2.4974	021, 201
22	3	2.8547	2.8530	120	1	<1	2.1318	2.1311	112
	8		2.8576	200		<1		2.1000	120
28	14	2.8432	2.8411	021	27	23	1.9892	1.9898	202, 022
10	5	2.8080	2.8105	002	3	1	1.9707	1.9706	211, 121
3	2	2.6235	2.6214	210	2	<1	1.9007	1.9009	003
	<1		2.5850	012		<1		1.8520	300
	3		2.5756	201	1	1	1.7984	1.7985	103, 013
62	47	2.5596	2.5580	121	2	2	1.7612	1.7615	301, 031
	3		2.5495	102	2	2	1.6907	1.6909	122, 212
14	4	2.5330	2.5304	$12\bar{1}$	1	1	1.6349	1.6353	113
	1		2.5200	$20\bar{1}$	17	16	1.6038	1.6039	220
37	22	2.4929	2.4955	$10\bar{2}$	12	8	1.5690	1.5688	203, 023
3	3	2.3999	2.3986	211		<1		1.5531	302, 032
1	1	2.3768	2.3775	112	20	11	1.5439	1.5440	221
1	1	2.3535	2.3536	$21\bar{1}$		<1		1.5410	130
	<1		2.3336	$11\bar{2}$	1	<1	1.4873	1.4876	311, 131
1	<1	2.1594	2.1582	220	1	<1	1.4259	1.4256	004
1	<1	2.1379	2.1377	022	1	3	1.4091	1.4093	213, 123
2	1	2.0452	2.0491	130	6	3	1.3980	1.3979	222
	<1		2.0447	031	3	1	1.3895	1.3890	400
17	5	2.0304	2.0314	202		<1		1.3809	104, 014
	13		2.0287	221	2	1	1.3556	1.3557	312, 132
	<1		2.0158	122	12	5	1.3491	1.3496	401, 041
17	11	2.0016	2.0012	$22\bar{1}$	1	<1	1.3262	1.3265	303, 033
	<1		1.9888	$12\bar{2}$	1	<1	1.3030	1.3028	114
8	7	1.9776	1.9773	$20\bar{2}$	1	<1	1.2752	1.2746	230
2	2	1.9417	1.9411	212	11	4	1.2685	1.2684	204, 024
3	1	1.9318	1.9312	131	5	3	1.2488	1.2487	402, 042
	<1		1.9192	$13\bar{1}$		<1		1.2440	321, 231
3	3	1.9049	1.9051	300	4	2	1.2258	1.2258	223
1	1	1.8945	1.8938	$21\bar{2}$		<1		1.2124	140

Raman spectroscopy

Raman spectroscopic analysis was performed with a HORIBA HR320 spectrometer using a 50 mW, 514.5 nm argon laser. Raman shifts were calibrated using silicon and the resulting spectra are shown in Fig. 2. Although signals were weak, several peaks could be distinguished. Based on comparisons with the spectra of related material (kapellasite and tondiite; Krause *et al.*, 2006; Malcherek *et al.*, 2014), peaks in the region below 500 cm^{-1} are thought to be derived from metal–anion stretching vibrations, while those in the region 3400–3600 cm^{-1} are attributed to O–H stretching. No peaks were found between 1200 and 1800 cm^{-1} in the spectra of both minerals, indicating the absence of H–O–H bending vibrations.

https://doi.org/10.1180/minmag.2016.080.104 Published online by Cambridge University Press

TABLE 3. Data collection information and structural refinement details for iyoite and misakiite.

	Iyoite	Misakiite
Temperature	298 K	
Radiation	Mo*K*α (λ = 0.71075 Å)	
Diffractometer	R-AXIS RAPID II	
Voltage, current	50 kV, 24 mA	
Structure solution	*Superflip*	
Refinement	Full-matrix least-squares on F^2	
Crystal size (mm)	0.07 × 0.02 × 0.01	0.06 × 0.06 × 0.03
Space Group	$P2_1/m$	$P3m1$
Unit-cell dimensions	a = 5.7208(8) Å b = 6.6045(7) Å c = 5.6224(7) Å β = 88.363(4)° V = 212.34(4) Å^3	a = 6.4168(4) Å c = 5.7099(4) Å V = 203.61(2) Å^3
Z	2	1
$D_{calc.}$	3.195 g cm^{-3}	3.413 g cm^{-3}
F(000)	195	200
Absorption coefficient, μ	8.29 mm^{-1}	9.88 mm^{-1}
2θ max	60°	60°
No. of reflections	4674	2388
Independent reflections	670	251
Reflections ($I > 2\sigma(I)$)	595	228
No. of LS parameters	43	19
Residuals: *R*int	0.035	0.041
Residuals: *R*1 ($I > 2\sigma(I)$)	0.019	0.025
Residuals: *R* (All data)	0.022	0.027
Residuals: *wR*2 (All data)	0.039	0.068
Goof	1.12	1.17
Largest diff. peak and hole	0.63 and –0.51 *e* Å^{-3}	0.96 and –0.75 *e* Å^{-3}

Chemical composition

Table 1 presents the chemical compositions of iyoite and misakiite, as determined using a JEOL JSM-5600 electron microprobe (energy-dispersive spectroscopy (EDS) mode, 15 kV, 0.4 nA, 5 μm beam diameter). Attempts with wavelength-dispersive spectroscopy mode at a higher beam current were unsuccessful due to electron damage, therefore we used the EDS mode with a broad beam in order to minimize sample damage. Although the presence of OH was confirmed by Raman spectroscopy and single-crystal X-ray diffraction, the proportions of water provided in Table 1 are calculated on a stoichiometric basis because insufficient material was available for direct determination of OH. The resulting empirical and simplified formula for iyoite (based on 4 anions per formula unit) are $Mn_{1.085}Cu_{0.915}Cl_{1.058}(OH)_{2.942}$ and $MnCuCl(OH)_3$, while those for misakiite (based on 8 anions per formula unit) are $Cu_{2.826}Mn_{1.174}(OH)_{5.900}Cl_{2.100}$ and $Cu_3Mn(OH)_6Cl_2$, respectively.

X-ray crystallography

Powder diffraction

The powder X-ray diffraction (XRD) patterns of the minerals were collected using a synchrotron X-ray source on the NE1 beam line of PF–AR, KEK, Japan, which provided a 30 μm diameter collimated beam of monochromatized X-ray radiation (λ = 0.4177 Å). XRD spectra were collected by the Debye–Scherrer method and recorded using an image plate detector, then converted to conventional one dimensional diffraction patterns using the *IPAnalyzer* and *PDindexer* software packages (Seto *et al.*, 2010). The resulting patterns are presented in Fig. 3 and derived *d* spacings and

https://doi.org/10.1180/minmag.2016.080.104 Published online by Cambridge University Press

TABLE 4. Final atom coordinates and displacement parameters (Å^2) for iyoite.

	x/a	*y/b*	*z/c*	U_{iso}*/U_{eq}	Occupancy	
Mn1	0.47495 (6)	1/4	−0.01353 (6)	0.01534 (11)	$Mn_{0.957(3)}Cu_{0.043(3)}$	
Cu2	1/2	0	1/2	0.01356 (9)	$Cu_{0.877(3)}Mn_{0.123(3)}$	
Cl1	0.14598 (10)	1/4	0.31130 (11)	0.02303 (15)	Cl	
O1	0.6468 (3)	1/4	0.6273 (3)	0.0156 (3)	O	
O2	0.6563 (2)	0.01796 (17)	0.1854 (2)	0.0156 (2)	O	
H1	0.798 (6)	1/4	0.619 (5)	0.021 (8)*	H	
H2	0.801 (4)	0.033 (3)	0.199 (4)	0.019 (5)*	H	
	U^{11}	U^{22}	U^{33}	U^{12}	U^{13}	U^{23}
Mn1	0.0243 (2)	0.01024 (18)	0.01151 (19)	0	−0.00048 (13)	0
Cu2	0.02016 (16)	0.01115 (15)	0.00929 (15)	−0.00127 (10)	0.00085 (11)	−0.00118 (9)
Cl1	0.0167 (3)	0.0281 (3)	0.0242 (3)	0	0.0008 (2)	0
O1	0.0179 (8)	0.0145 (8)	0.0143 (8)	0	0.0016 (6)	0
O2	0.0161 (6)	0.0163 (6)	0.0144 (6)	−0.0009 (4)	−0.0011 (5)	−0.0008 (4)

* refined with isotropic displacement parameters.

reflection intensities data are listed in Table 2. The unit-cell parameters refined from the powder data for iyoite ($P2_1/m$) are a = 5.717(2), b = 6.586(2), c = 5.623(3) Å, β = 88.45(3)° and V = 211.63(15) Å^3, while those for misakiite ($P\bar{3}m1$) are a = 6.4156(4), c = 5.7026(5) Å and V = 203.27(3) Å^3.

TABLE 5. Selected bond distances (Å) and angles (°) in iyoite.

Mn1–O1^{iv}	2.2207 (17)	Cu2–O1	1.9946 (10)
Mn1–O2	2.1776 (12)	Cu2–O1^{v}	1.9946 (10)
Mn1–O2^{i}	2.1612 (11)	Cu2–O2^{v}	1.9628 (12)
Mn1–O2^{ii}	2.1612 (11)	Cu2–O2	1.9628 (12)
Mn1–O2^{iii}	2.1776 (12)	Cu2–Cl1	2.8419 (5)
Mn1–Cl1	2.5847 (7)	Cu2–Cl1^{v}	2.8419 (5)
O1–H1	0.87 (3)	O2–H2	0.84 (2)
O2^{i}–Mn1–O2^{ii}	109.95 (6)	O1^{v}–Cu2–Cl1	92.01 (4)
O2^{i}–Mn1–O2^{iii}	169.29 (4)	O2^{v}–Cu2–Cl1^{v}	86.54 (4)
O2^{ii}–Mn1–O2^{iii}	80.21 (5)	O2–Cu2–Cl1^{v}	93.46 (4)
O2^{i}–Mn1–O2	80.21 (5)	O1–Cu2–Cl1^{v}	92.01 (4)
O2^{ii}–Mn1–O2	169.29 (4)	O1^{v}–Cu2–Cl1^{v}	87.99 (4)
O2^{iii}–Mn1–O2	89.46 (6)	Cl1–Cu2–Cl1^{v}	180
O2^{i}–Mn1–O1^{iv}	75.17 (4)		
O2^{ii}–Mn1–O1^{iv}	75.17 (4)		
O2^{iii}–Mn1–O1^{iv}	105.18 (5)		
O2–Mn1–O1^{iv}	105.18 (5)		
O2^{i}–Mn1–Cl1	93.47 (4)		
O2^{ii}–Mn1–Cl1	93.47 (4)		
O2^{iii}–Mn1–Cl1	89.15 (4)		
O2–Mn1–Cl1	89.15 (4)		
O1^{iv}–Mn1–Cl1	159.57 (5)		

Symmetry codes: (i) −x+1, −y, −z; (ii) −x+1, y+1/2, −z; (iii) x, −y+1/2, z; (iv) x, y, z−1; (v) −x+1, −y, −z+1.

https://doi.org/10.1180/minmag.2016.080.104 Published online by Cambridge University Press

TABLE 6. Final atom coordinates and displacement parameters (Å^2) for misakiite.

	x/*a*	*y*/*b*	*z*/*c*	U_{iso}*/U_{eq}	Occupancy
Cu1	1/2	0	1/2	0.0116 (2)	$Cu_{0.94}Mn_{0.06}$
Mn2	0	0	1/2	0.0147 (3)	Mn
Cl1	1/3	2/3	0.1405 (2)	0.0205 (3)	Cl
O	0.3615 (4)	0.18073 (19)	0.3467 (4)	0.0129 (5)	O
H	0.393 (10)	0.196 (5)	0.210 (10)	0.032 (14)*	H
	U^{11}	U^{22}	U^{33}	U^{12}	U^{13}	U^{23}
Cu1	0.0081 (3)	0.0098 (3)	0.0174 (3)	0.00491 (14)	0.00108 (8)	0.00216 (16)
Mn2	0.0095 (4)	0.0095 (4)	0.0250 (6)	0.00477 (18)	0	0
Cl1	0.0235 (4)	0.0235 (4)	0.0145 (6)	0.0118 (2)	0	0
O	0.0136 (10)	0.0118 (8)	0.0140 (11)	0.0068 (5)	0.0013 (8)	0.0006 (4)

* refined with isotropic displacement parameters.

Single-crystal diffraction

Single-crystal XRD analyses of both minerals were carried out using a Rigaku R-AXIS RAPID II diffractometer equipped with a curved imaging plate and employing monochromatized Mo*K*α radiation. The Rigaku *RAPID AUTO* software package was used for the processing of diffraction

TABLE 7. Selected bond distances (Å) and angles (°) for misakiite.

Cu1–O1^{i}	1.9830 (14)	Mn2–O1^{vi}	2.191 (2)
Cu1–O1	1.9830 (14)	Mn2–O1^{vii}	2.191 (2)
Cu1–O1^{ii}	1.9830 (14)	Mn2–O1^{viii}	2.191 (2)
Cu1–O1^{iii}	1.9831 (14)	Mn2–O1	2.191 (2)
Cu1–Cl1^{iv}	2.7649 (10)	Mn2–O1^{ix}	2.191 (2)
Cu1–Cl1^{v}	2.7649 (10)	Mn2–O1^{iii}	2.191 (2)
O1–H1	0.80 (6)		
O1^{i}–Cu1–O1	180	O1^{vi}–Mn2–O1^{vii}	105.11 (7)
O1^{i}–Cu1–O1^{ii}	84.42 (13)	O1^{vi}–Mn2–O1^{viii}	180.000 (1)
O1–Cu1–O1^{ii}	95.58 (13)	O1^{vii}–Mn2–O1^{viii}	74.89 (7)
O1^{i}–Cu1–O1^{iii}	95.58 (13)	O1^{vi}–Mn2–O1	105.11 (7)
O1–Cu1–O1^{iii}	84.42 (13)	O1^{vii}–Mn2–O1	105.11 (7)
O1^{ii}–Cu1–O1^{iii}	180	O1^{viii}–Mn2–O1	74.89 (7)
O1^{i}–Cu1–Cl1^{iv}	90.66 (6)	O1^{vi}–Mn2–O1^{ix}	74.89 (7)
O1–Cu1–Cl1^{iv}	89.33 (6)	O1^{vii}–Mn2–O1^{ix}	74.89 (7)
O1^{ii}–Cu1–Cl1^{iv}	89.34 (6)	O1^{viii}–Mn2–O1^{ix}	105.11 (7)
O1^{iii}–Cu1–Cl1^{iv}	90.66 (6)	O1–Mn2–O1^{ix}	180
O1^{i}–Cu1–Cl1^{v}	89.34 (6)	O1^{vi}–Mn2–O1^{iii}	74.89 (7)
O1–Cu1–Cl1^{v}	90.67 (6)	O1^{vii}–Mn2–O1^{iii}	180.000 (1)
O1^{ii}–Cu1–Cl1^{v}	90.66 (6)	O1^{viii}–Mn2–O1^{iii}	105.11 (7)
O1^{iii}–Cu1–Cl1^{v}	89.34 (6)	O1–Mn2–O1^{iii}	74.89 (7)
Cl1^{iv}–Cu1–Cl1^{v}	180	O1^{ix}–Mn2–O1^{iii}	105.11 (7)

Symmetry codes: (i) −x+1, −y, −z+1; (ii) −y+1, x−y, z; (iii) y, −x+y, −z+1; (iv) −x+1, −y+1, −z+1; (v) x, y−1, z; (vi) −x+y, −x, z; (vii) −y, x−y, z; (viii) x−y, x, −z+1; (ix) −x, −y, −z+1.

https://doi.org/10.1180/minmag.2016.080.104 Published online by Cambridge University Press

data, including the application of a numerical absorption correction. The structures were solved by the charge-flipping method using *Superflip* (Palatinus and Chapuis, 2007). The *SHELXL-97* software package (Sheldrick, 2008) was used for structure refinement. Scattering factors for neutral atoms and coefficients for X-ray dispersion corrections were taken from the *International Tables for Crystallography* (Wilson, 1992). All non-hydrogen atom positions were located by the charge-flipping method. All hydrogen atoms were revealed by difference-Fourier maps. Positions and isotropic displacement parameters of hydrogen atoms were refined freely without imposing constraints. Data collection information and structural refinement details for the two minerals are provided in Table 3. Final atom coordinates with displacement parameters and selected bond distances and angles for iyoite are summarized in Tables 4 and 5. Those for misakiite are listed in Tables 6 and 7.

Iyoite, $MnCuCl(OH)_3$, was determined to be isostructural with botallackite, $Cu_2Cl(OH)_3$. Although iyoite has an unconventional axial setting of $\beta < 90°$, we chose this in order to facilitate comparison, as shown in Fig. 4. It is evident that the monoclinic distortion is reversed between iyoite and botallackite. Subsequently, we examined the occupancy of Mn and Cu at the cation site using the composition from EDS results. In the disordered model with $Mn_{0.54}Cu_{0.46}$ occupancy in both cation sites, R converged to $R_1 = 4.0\%$. On the other hand, the occupancy refinement yields a smaller R factor ($R_1 = 1.9\%$) with the Mn-Cu ordered structure. The refinement yields $Mn_{0.957(3)}Cu_{0.043(3)}$ at the Mn1 site and $Cu_{0.877(3)}Mn_{0.123(3)}$ at the Cu2 site; thus Mn and Cu are apparently ordered in iyoite (Table 4). This is the first time that ordering of another metal has been shown to occur in the botallackite structure. The Mn1 site in iyoite is octahedrally coordinated by five hydroxyl ions and one chloride, and the $Mn(OH)_5Cl$ octahedron is irregularly distorted (Table 5). The Cu2 site is also octahedrally coordinated by four hydroxyl ions and two chlorides, and the distortion of the $Cu(OH)_4Cl_2$ octahedron is remarkably Jahn-Teller distorted (Table 5). The whole structure is based on brucite-like sheets parallel to {100} and built from edge-sharing, distorted $Mn(OH)_5Cl$ and Jahn-Teller distorted $Cu(OH)_4Cl_2$ octahedra (Fig. 5). The sheets are connected *via* weak interplanar O–H···Cl bonds.

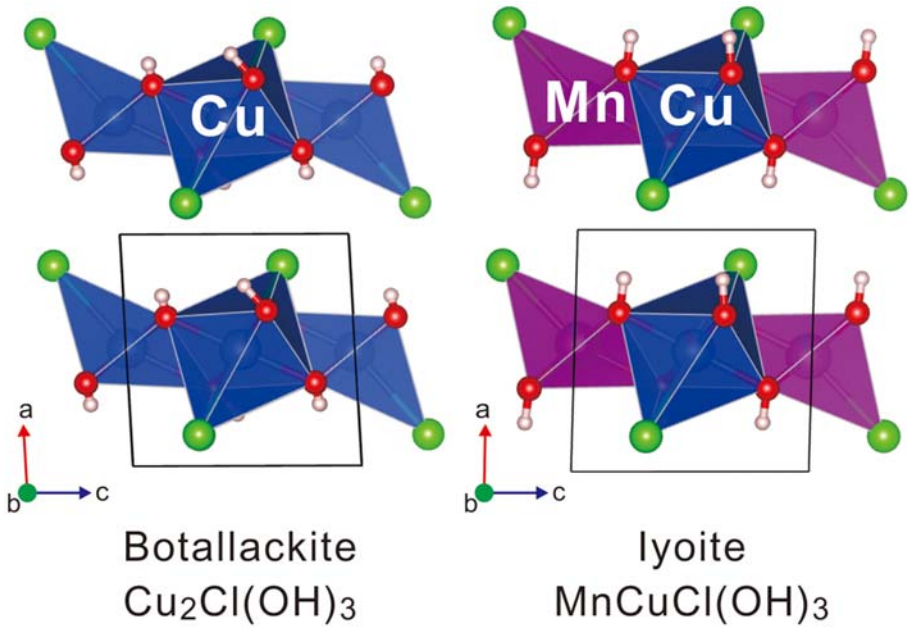

FIG. 4. Comparison between botallackite (Hawthorne, 1985) and iyoite (this study). These two minerals are isostructural, although the monoclinic distortion is opposite and the cations are ordered in iyoite. Even though the axial setting of iyoite is unconventional with $\beta < 90°$, it was chosen in order to allow comparison.

https://doi.org/10.1180/minmag.2016.080.104 Published online by Cambridge University Press

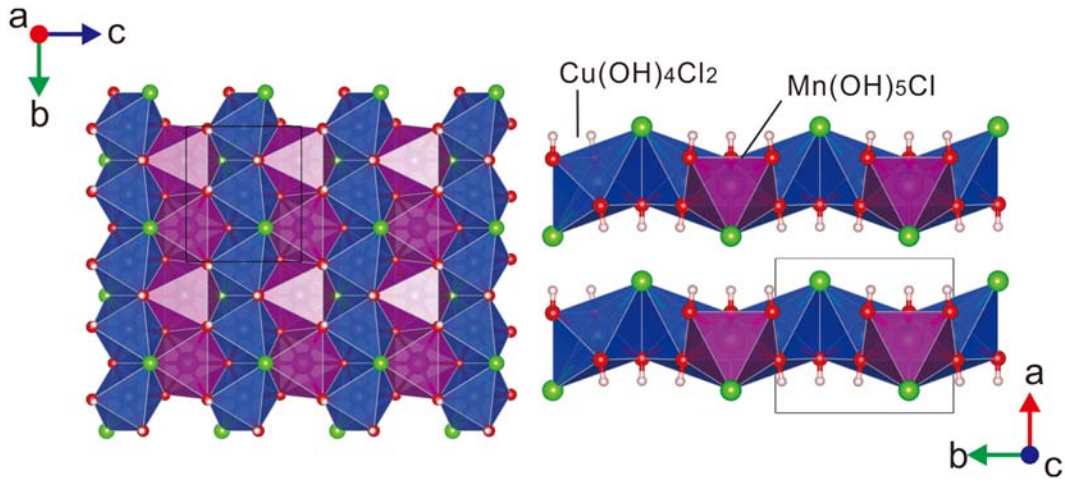

FIG. 5. Crystal structure of iyoite. The structure is based on brucite-like sheets parallel to {100} built from edge-sharing, distorted $Mn(OH)_5Cl$ and Jahn-Teller-distorted $Cu(OH)_4Cl_2$ octahedral layers. The sheets stack directly on one another and bond to adjacent sheets *via* weak hydrogen and O···Cl bonds.

The results obtained for misakiite are summarized in Tables 6 and 7. Refinement of site occupancies (Mn *vs.* Cu) gave an ordered Mn-Cu structure (R_1 = 2.5%), while the disordered model produced a significantly larger *R* factor (R_1 = 6.3%). Consequently, it is clear that misakiite, $Cu_3Mn(OH)_6Cl_2$, corresponds to an Mn-rich analogue of kappellasite, $Cu_3Zn(OH)_6Cl_2$. The Cu1 site in misakiite is octahedrally coordinated by four hydroxyls and two chlorines, and the distortion of the $Cu(OH)_4Cl_2$ octahedron is remarkable in the copper-chlorine bond direction (Table 5). Whereas the Mn2 site is octahedrally coordinated by six hydroxyl ions, and the $Mn(OH)_6$ octahedron exhibits different bond angles (Table 5). Its structure is also based on brucite-like sheets parallel to {001}, built from edge-sharing, angle-distorted $Mn(OH)_6$ and Jahn-Teller distorted $Cu(OH)_4Cl_2$ octahedra (Fig. 6). In this structure, $Mn(OH)_6$ and $Cu(OH)_4Cl_2$ octahedra form a triangular lattice and a kagome lattice in the sheets, respectively. The sheets are also minimally linked by weak

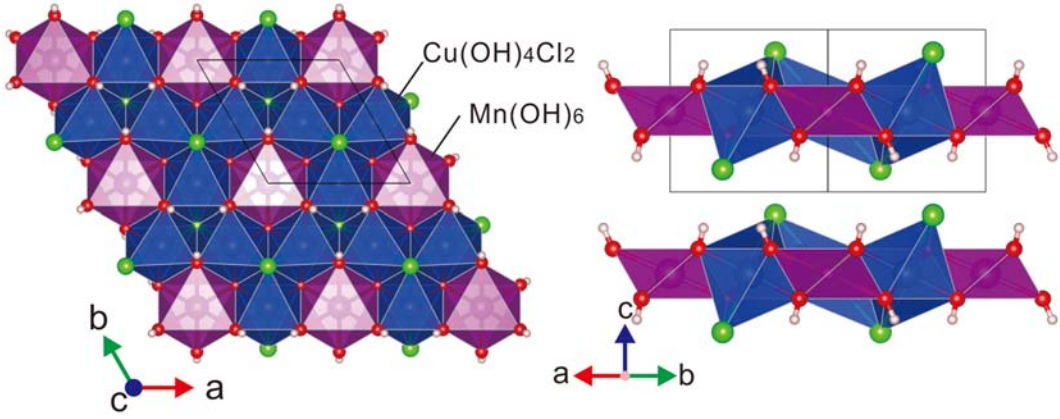

FIG. 6. Crystal structure of misakiite. The structure is also based on brucite-like sheets parallel to {001} built from edge-sharing angle-distorted $Mn(OH)_6$ and Jahn-Teller distorted $Cu(OH)_4Cl_2$ octahedra. $Mn(OH)_6$ and $Cu(OH)_4Cl_2$ octahedra form triangles and a kagome lattice in the sheet, respectively.

https://doi.org/10.1180/minmag.2016.080.104 Published online by Cambridge University Press

TABLE 8. Comparable data for the atacamite family.

Structure type (space group)	Mineral	Composition	*a* (Å)	*b* (Å)	*c* (Å)	α (°)	β (°)	γ (°)	*V* (Å^3)	Reference
3D framework (*Pnma*)	Atacamite	$Cu_2Cl(OH)_3$	6.030	6.865	9.120	90	90	90	377.5	Parise and Hyde (1986)
	Kempite[1]	$Mn_2Cl(OH)_3$	6.49	7.11	9.52	90	90	90	439.3	Zenmyo *et al.* (2011)
	Hibbingite[2]	$Fe_2Cl(OH)_3$	6.31	7.10	9.20	90	90	90	412.2	Saini-Eidukat *et al.* (1994)
3D framework ($P2_1/n$)	Clinoatacamite	$Cu_2Cl(OH)_3$	6.144	6.805	9.112	90	99.55	90	375.7	Grice *et al.* (1996)
3D framework (*R*3)	Paratacamite	$Cu_3(Cu,Zn)(OH)_6Cl_2$	13.654	= *a*	14.041	90	90	120	2267.0	Fleet (1975)
	Paratacamite-(Ni)	$Cu_3Ni(OH)_6Cl_2$	13.682	= *a*	13.916	90	90	120	2256.0	Sciberras *et al.* (2014)
	Paratacamite-(Mg)	$Cu_3Mg(OH)_6Cl_2$	13.689	= *a*	14.025	90	90	120	2275.8	Kampf *et al.* (2013*a*)
3D framework (*R*3 m)	Herbertsmithite	$Cu_3Zn(OH)_6Cl_2$	6.834	= *a*	14.075	90	90	120	569.3	Braithwaite *et al.* (2004)
	Gillardite	$Cu_3NiCl_2(OH)_6$	6.836	= *a*	13.846	90	90	120	560.4	Clissold *et al.* (2007)
	Leverettite	$Cu_3CoCl_2(OH)_6$	6.844	= *a*	14.064	90	90	120	570.4	Kampf *et al.* (2013*b*)
	Tondiite	$Cu_3MgCl_2(OH)_6$	6.838	= *a*	14.088	90	90	120	570.4	Malcherek *et al.* (2014)
Layer ($P2_1/m$)	Botallackite	$Cu_2Cl(OH)_3$	5.717	6.126	5.636	90	93.07	90	197.1	Hawthorne (1985)
	Iyoite	$MnCuCl(OH)_3$	5.717	6.586	5.623	90	88.45	90	211.6	This study
Layer (*P*3*m*1)	Kapellasite	$Cu_3Zn(OH)_6Cl_2$	6.300	= *a*	5.733	90	90	120	197.1	Krause *et al.* (2006)
	Haydeeite	$Cu_3Mg(OH)_6Cl_2$	6.273	= *a*	5.747	90	90	120	195.9	Malcherek and Schlüter (2007)
	Misakiite	$Cu_3Mn(OH)_6Cl_2$	6.416	= *a*	5.703	90	90	120	203.3	This study

[1]Synthetic sample. [2]Axis transformation form *Pnam* inferred by Saini-Eidukat *et al.* (1994).

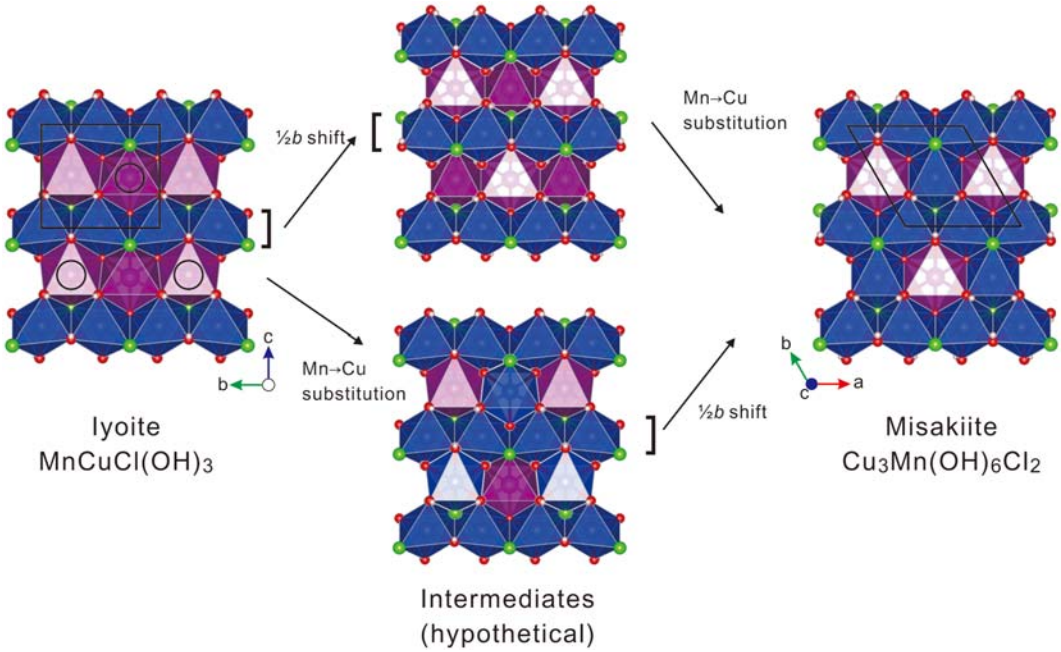

FIG. 7. Comparison of iyoite and misakiite structures. The misakiite structure can be derived from that of iyoite by a 1/2*b* shift of the iyoite $Cu(OH)_4Cl_2$ layer and Mn-Cu substitution at the triangular positions as indicated by circles.

interplanar O–H···Cl bonds, just as in the iyoite structure.

Structural relationship

As noted, the atacamite family contains two general stoichiometries, $M_2Cl(OH)_3$ and $Cu_3M(OH)_6Cl_2$. The structures in the atacamite family can be divided into two different types of three-dimensional frameworks and layer structures (Table 8). The latter is represented by botallackite and kapellasite, and the new minerals described herein correspond to their structural analogues. Iyoite and misakiite occur in close association with each other, probably due to the close structural and compositional relationships between the two minerals. In the present study, we generated the structures of both minerals using *VESTA* to allow for comparison (Momma and Izumi, 2011). The iyoite structural sheet consists of edge-sharing Cu $(OH)_4Cl_2$ and $Mn(OH)_5Cl$ octahedral layers that are alternately stacked along the *c* axis (Fig. 7). In contrast, the misakiite structural sheets are composed of $Mn(OH)_6$ at triangular lattice positions and $Cu(OH)_4Cl_2$ at kagome lattice positions. Thus, the misakiite structure can be derived from that of iyoite by a 1/2*b* shift of the iyoite $Cu(OH)_4Cl_2$ layer and an Mn-Cu substitution at the triangular lattice positions (Fig. 7).

Synthesis

There are several reports of the synthesis of layer-structured minerals in the atacamite family, specifically botallackite, kapellasite and haydeeite (Pollard *et al.*, 1989; Zheng and Xu, 2004; Colman *et al.*, 2010), but synthesis of the iyoite and misakiite compounds has never been reported. We attempted to synthesize these new minerals using previously reported hydrothermal methods used for botallackite, kapellasite and haydeeite. However, only misakiite was successfully produced using a hydrothermal method. In these trials, metallic copper (0.05 g), $MnCl_2{\cdot}4H_2O$ (1.8 g) and 30% H_2O_2 (2.0 ml) were combined in a 30 cm^3 Teflon beaker held at 253 K. The beaker was then placed in a stainless steel autoclave and heated at 433 K for 80 hours. The product included a rosette of aggregated, hexagonal, green, platy crystals (Fig. 8), the chemical composition and Raman spectrum of which were consistent with misakiite (Table 1; Fig. 2). Although the structural refinement of single-

https://doi.org/10.1180/minmag.2016.080.104 Published online by Cambridge University Press

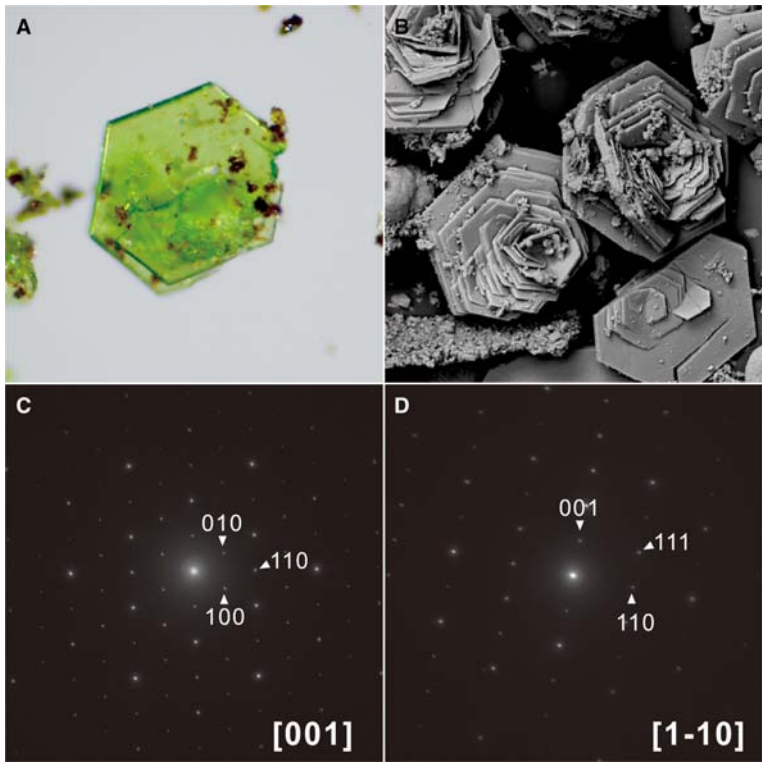

FIG. 8. (*a*) Micrograph and (*b*) scanning electron microscopic image of synthetic misakiite and selected-area electron diffraction patterns from the (*c*) [001] and (*d*) [1$\bar{1}$0] ones. The field of view is 0.1 mm in (*a*) and (*b*).

crystal X-ray data did not converge due to the mosaicity of the crystals, the unit-cell parameters determined by transmission electron diffraction (a = 6.4 and c = 5.7 Å) were comparable to those of misakiite. Unfortunately, the synthesis of iyoite was not successful. Although iyoite coexists with misakiite in Nature, its optimal synthetic conditions may be narrower than those for misakiite, as the layer-structured atacamite family is thought to be inherently of low thermal stability (Pollard *et al.*, 1989; Krause *et al.*, 2006). Nevertheless, the formation of iyoite and misakiite in Nature evidently occurs, as the present minerals were probably formed by the reaction between seawater and manganese ore including native copper.

Acknowledgements

Powder XRD data were acquired at KEK (Proposal no. 2013G540). The authors are also grateful to the anonymous referees of this manuscript for their constructive reviews.

References

Braithwaite, R.S.W., Mereiter, K., Paar, W.H. and Clark, A.M. (2004) Herbertsmithite, $Cu_3Zn(OH)_6Cl_2$, a new species, and the definition of paratacamite. *Mineralogical Magazine*, **68**, 527–539.

Clissold, M.E., Leverett, P., Williams, P.A., Hibbs, D.E. and Nickel, E.H. (2007) The structure of gillardite, the Ni-analogue of herbertsmithite, from Widgiemooltha, Western Australia. *The Canadian Mineralogist*, **45**, 317–320.

Colman, R.H., Sinclair, A. and Wills, A.S. (2010) Comparisons between haydeeite, α-$Cu_3Mg(OD)_6Cl_2$, and kapellasite, α-$Cu_3Zn(OD)_6Cl_2$, isostructural S = 1/2 Kagome Magnets. *Chemistry of Materials*, **22**, 5774–5779.

Fleet, M.E. (1975) Crystal-structure of paratacamite, $Cu_2(OH)_3Cl$. *Acta Crystallographica*, **B31**, 183–187.

Grice, J.D., Szymansk, i J.T. and Jambor, J.L. (1996) Crystal structure of clinoatacamite, a new polymorph of $Cu_2(OH)_3Cl$. *The Canadian Mineralogist*, **34**, 61–72.

Hawthorne, F.C. (1985) Refinement of the crystal-structure of botallackite. *Mineralogical Magazine*, **49**, 87–89.

https://doi.org/10.1180/minmag.2016.080.104 Published online by Cambridge University Press

Kampf, A.R., Sciberras, M.J., Leverett, P., Williams, P.A., Malcherek, T., Schlüter, J., Welch, M.D., Dini, M. and Molina Donoso, A.A. (2013*a*) Paratacamite-(Mg), Cu3(Mg,Cu)Cl2(OH)6; a new substituted basic copper chloride mineral from Camerones, Chile. *Mineralogical Magazine,* **77,** 3113–3124

Kampf, A.R., Sciberras, M.J., Williams, P.A., Dini, M. and Donoso, A.A.M. (2013*b*) Leverettite from the Torrecillas mine, Iquique Provence, Chile: the Co-analogue of herbertsmithite. *Mineralogical Magazine*, **77**, 3047–3054.

Krause, W., Bernhardt, H.J., Braithwaite, R.S.W., Kolitsch, U. and Pritchard, R. (2006) Kapellasite, $Cu_3Zn(OH)_6Cl_2$, a new mineral from Lavrion, Greece, and its crystal structure. *Mineralogical Magazine*, **70**, 329–340.

Malcherek, T. and Schlüter, J. (2007) $Cu_3MgCl_2(OH)_6$ and the bond-valence parameters of the OH–Al bond. *Acta Crystallographica*, **B63**, 157–160.

Malcherek, T., Bindi, L., Dini, M., Ghiara, M.R., Molina Donoso, A., Nestola, F., Rossi, M. and Schlüter, J. (2014) Tondiite, $Cu_3Mg(OH)_6Cl_2$, the Mg-analogue of herbertsmithite. *Mineralogical Magazine*, **78**, 583–590.

Momma, K. and Izumi, F. (2011) VESTA 3 for three-dimensional visualization of crystal, volumetric and morphology data. *Journal of Applied Crystallography*, **44**, 1272–1276.

Nozaki, T., Kato, Y. and Suzuki, K. (2013) Late Jurassic ocean anoxic event: evidence from voluminous sulphide deposition and preservation in the Panthalassa. *Scientific Reports*, **3**, 1889.

Parise, J.B. and Hyde, B.G. (1986) The structure of atacamite and its relationship to spinel. *Acta Crystallographica*, **C42**, 1277–1280.

Palatinus, L. and Chapuis, G. (2007) SUPERFLIP – a computer program for the solution of crystal structures by charge flipping in arbitrary dimensions. *Journal of Applied Crystallography*, **40**, 786–790.

Pollard, A.M., Thomas R.G. and Williams P.A. (1989) Synthesis and stabilities of the basic copper(II) chlorides atacamite, paratacamite and botallackite. *Mineralogical Magazine*, **53**, 557–563.

Rogers, A.F. (1924) Kempite, a new manganese mineral from California. *American Journal of Science*, **8**, 145–150.

Saini-Eidukat, B., Kucha, H. and Keppler, H. (1994) Hibbingite, γ-$Fe_2(OH)_3Cl$, a new mineral from the Duluth Complex, Minnesota, with implications for the oxidation of Fe-bearing compounds and the transport of metals. *American Mineralogist*, **79**, 555–561.

Sciberras, M.J., Leverett, P., Williams, P.A., Hibbs, D.E., Malcherek, T., Schlüter, J., Welch, M., Downes, P.J. and Kampf, A.R. (2014) Paratacamite-(Ni), $Cu_3(Ni, Cu)Cl_2(OH)_6$, a new mineral from the Carr Boyd Rocks mine, Western Australia. *Australian Journal of Mineralogy*, **17**, 39–44.

Seto, Y., Nishio-Hamane, D., Nagai, T. and Sata, N. (2010) Development of a software suite on X-ray diffraction experiments. *Review of High Pressure Science and Technology*, **20**, 269–276.

Sheldrick, G.M. (2008) A short history of SHELX. *Acta Crystallographica*, **A64**, 112–122.

Wilson, A.J.C. (1992) *International Tables for Crystallography Volume C.* Kluwer, Dordrecht, The Netherlands.

Zenmyo, K., Kubo, H., Tokita, M., Hamasaki, T., Hagihala, M. and Zheng, X-G. (2011) Proton NMR study of pyrochlore-like atacamite $Mn_2Cl(OH)_3$. *Journal of the Physical Society of Japan,* **80,** 024704.

Zheng, X.G. and Xu, C.N. (2004) Antiferromagnetic transition in botallackite $Cu_2Cl(OH)_3$. *Solid State Communications*, **131**, 509–511.

https://doi.org/10.1180/minmag.2016.080.104 Published online by Cambridge University Press